# Marked Point Process for Vascular Tree Extraction on Angiogram

Kaiqiong Sun, Nong Sang, and Tianxu Zhang

Institute for Pattern Recognition and Artificial Intelligence
Huazhong University of Science and Technology, Wuhan 430074, P.R. China
kqsunn@gmail.com,{nsang,txzhang}@hust.edu.cn

**Abstract.** This paper presents a two-step algorithm to perform automatic extraction of vessel tree on angiogram. Firstly, the approximate vessel centerline is modeled as marked point process with each point denoting a line segment. A *Double Area* prior model is proposed to incorporate the geometrical and topological constraints of segments through potentials on the interaction and the type of segments. Data likelihood allows for the vesselness of the points which the segment covers, which is computed through the Hessian matrix of the image convolved with 2-D Gaussian filter at multiple scales. Optimization is realized by simulated annealing scheme using a Reversible Jump Markov Chain Monte Carlo (RJMCMC) algorithm. Secondly, the extracted approximate vessel centerline, containing global geometry shape as well as location information of vessel, is used as important guide to explore the accurate vessel edges by combination with local gradient information of angiogram. This is implemented by morphological homotopy modification and watershed transform on the original gradient image. Experimental results of clinical digitized coronary angiogram are reported.

**Keywords:** Angiogram, Vascular tree, Segmentation, Stochastic geometry, Marked point process, Markov Chain Monte Carlo.

## 1 Introduction

Vessel segmentation algorithm is critical component of circulatory blood vessel analysis systems. It provides important information of quantitative analysis about cardiac and cerebral disease. The difficulties of vessel segmentation mainly come from the weak contrast between vascular trees and the background, an advance unknown and easily deformable shapes of the vessel tree, sometimes overlapping strong shadows of bones and so on.

Many techniques about the problem of coronary vessel extraction begin with some local optimization process to character the vessel structure in the form of different description, operator and model. They have been built upon the pixel domain and different feature spaces of image. Region growing techniques mainly discriminate the vessel part from angiogram by intensity similarity and spatial proximity. Skeleton-based methods aim at extracting blood vessel centerlines, from which the whole vessel tree is reconstructed [1]. The ridge-based methods

A.L. Yuille et al. (Eds.): EMMCVPR 2007, LNCS 4679, pp. 467–478, 2007.

make use of intensity ridges to approximate the skeleton of the tubular objects while the grays image is treated as 3D elevation maps [2]. Ridge points can be obtained by tracing the intensity map from arbitrary point, along the steepest ascent direction of intensity. The Hessian matrix, containing the second-order differential properties of image, are also been used to track the ridge point [3] [4]. Matching filter approach convolves the image with multiple matched filters for the extraction of vessel structure [5]. The essence of this method existing in describes or approaches local lattices of image with the convolution kernel used. This method compares to the mathematical morphology schemes, which apply structuring elements to "match" the image with morphologic operators. The combination of several operators has also been proposed to complement one or more of them. For the incompleteness of these local descriptions for vessel structure, they usually have a heuristic post-processing step.

The methods based on local process usually lack detailed description of the geometry and topology of the global vessel structure, and might be very sensitive to local minima. Thus, besides the local description of vessel structure, other methods for vessel segmentation have also been proposed to character some relation between the local feature and shape of the whole structure [6],[7]. These methods usually are expressed with some model. Deformable models are such techniques that find object contours using parametric curves that deform under the influence of internal and external forces. It can either be parametric [8] or geometric [9]. The curvature and the gradient, acting as description for shape and intensity feature of vessel structure, are used to define an energy function. The final contour fits the vessel boundaries following a differential equation whose solution corresponds to a local minimum of the energy. In these methods, the constraint for curvature can be treated as the prior information about the vessel structure.

The prior information about vessel, however, can also be embedded into some model for the region of vessel structure instead of the edges. Based on such consideration, a two-step method, which combines the global geometry and local operator, for vessel extraction is proposed to achieve both robustness and accuracy in this paper. The basic idea is to inference the global geometry information, the approximate vessel centerline, and makes use of it to regularize a local edge detection algorithm. Where the abstract geometry embodied in object acts as important carrier of detailed quantities information of object.

The stochastic geometry model is explored to capture the geometry and topology of vessel tree. Assume the vessel centerline consists of local linear segments with certainly length and orientation, which is called approximate vessel centerline. In the first step, approximate vessel centerline is modeled as marked point process [10]. A *Double Area* model is proposed to incorporate the geometric and topological knowledge of vessel structure. The connectivity of structure is characterized by distance of extreme point of segments. The orientation consistency of connected segment characters the alignment of vessel structure. The optimization is done via simulated annealing using a Reversible Jump Markov Chain Monte Carlo (RJMCMC) algorithm [11],[12]. We design well balanced

Markov chains to explore the solution space. Moreover, Data-Driven techniques are utilized to compute heuristic information in the cue space [13].

As some abstract geometric descriptor of vessel structure, the approximate centerline contains important shape and location information of vessel tree. Thus, in the second step, the centerline is used as important guide to explore the accurate vessel edges by combination with local gradient information of angiogram. This is implemented by morphological homotopy modification and watershed transform on the original gradient image.

Several contributions have been proposed for vessel extraction with point process under the stochastic geometry framework. A Gaussian intensity model developed by E.Thönnes et al. [14] is adopted and used as the observed data under a Bayesian framework. Vascular image is modeled with random tree models(RTMs). A multi-scale approach based on marked point processes is proposed in [15]. Compared with the existing object-orientated methods, the proposed method in this paper model the shape or geometry rather than the vessel object (region or edge) itself. It takes advantage of the point process in a mediate way for vessel extraction. The approximate centerline explored acts as a hidden variable [16], [17] in the sense of computing for vessel extraction. The robustness is assumed by the geometry model and the accuracy is kept for the local operator used.

This paper is organized as follows: In the next section, the Double Area model is described and used for modeling the approximate vessel centerline. Next, the RJMCMC dynamics is built to simulate the model. In section 3, experiments on simulation of the point process with real clinic x-ray angiogram are reported. Section 4 describes the process of watershed technology used to detect accuracy vessel boundaries with the extracted vessel approximate centerline as marker. Finally, some discussion is presented.

## 2 Model for Approximate Vessel Centerline Extraction

Among the stochastic methods widespread in image analysis, the marked point process has the advantage of combing information "globally" to identify geometrical shape and is acknowledged more appropriate prior model than discrete Markov random fields [18] to use in object recognition and some other "high-level" vision problem. It is adopted in order to solve image analysis problems using an object-oriented rather than a pixel-oriented approach [16]. In this section, we firstly turn the vessel segmentation into a shape recognition problem and make use of marked point process to model approximate vessel centerline, which contains the shape and topology information of vessel.

The approximate vessel centerline is described as a configuration of line segments set. A segment is given by $s_i = (p_i, m_i)$, with $p_i = (x_i, y_i) \in \wedge \subset R^2$, the coordinates of its center. The label of a segment $m_i = (l_i, \theta_i) \in \Omega_M$ are its length and orientation. $\wedge$ is the lattices the image covers. $\Omega_M$ is the marker space $[l_{min}, l_{max}] \times [0, \pi]$. The line segments set $S = \{s_i, i = 1, ..., n \in N\}$ is considered as a realization of a point process on $\wedge \times \Omega_M$.

The real vessel centerline is generally characterized by several strong constraints such as structure continuity and consistency of local orientation. These constrains can be considered as interactions between segments of the point process which can either penalize or favor some particular configuration through potentials in the density of process. Two components constitute the probability density of the point process. The first is the interaction model (Double Area model), which is determined by the interaction between segments: attraction, rejection, and the dimension of the segments set. The second term is the data model, which gives the location in the image of the different segment with the centerline.

Within the framework of a Gibbs point process [16], the probability density of the proposed model is:

$$f(S) \propto \beta^n \exp(-E(S)) = \beta^n exp - (E_p(S) + E_d(S)) \ , \tag{1}$$

where $E_p(S)$ is the interaction energy, and $E_d(S)$ is the data energy. The estimate of the approximate centerline is obtained by minimizing the energy function $E(S)$:

$$S^* = \arg\min\{E_p(S) + E_d(S) - n\log\beta\} \ . \tag{2}$$

The term $-n\log\beta$ is the energy term corresponding to the Poisson process to which the density of point process with respect, and may be interpreted as a penalty on the total number of segments.

The global minimum of the energy function $E(S)$ is found by a simulated annealing technique. This algorithm iteratively simulates the law:

$$f(S,T) = [f(S)]^{\frac{1}{T}} \ , \tag{3}$$

while slowly decreasing the temperature $T$. When $T \to 0$, the result of the simulations converges in probability to the global minimum.

### 2.1 Double Area Model

The Double Area model is based on the types of segments and two relations of interaction between segments, $R_a$ (attraction) and $R_r$ (rejection). The energy of this prior model is:

$$E_p(S) = \lambda_0 n + \lambda_1 n_f + \lambda_2 n_s + \lambda_a \sum_{<s_i,s_j>R_a} g_a(s_i,s_j) + \lambda_r \sum_{<s_i,s_j>R_r} g_r(s_i,s_j) \ . \tag{4}$$

In the above prior energy, $n$, $n_f$ and $n_s$ are respectively the number of total segments, free segments and single segments. $\lambda_0$, $\lambda_1$, and $\lambda_2$ are the penalty constant for the number of them. $\lambda_0$ is $-\log\beta$ in formula (2). We follow the definition of segment types in [19]; two segments are said to be connected if two of their extremities are closer than a constant $\epsilon$. This relation defines three types of segments. Free segments are those which are not connected, single ones are those with only one of their endpoints connected to other segments, and double segments have their two endpoints connected.

$< s_i, s_j > R_a$ is a pair of interacting segments of attraction, and $g_a(s_i, s_j)$ is the potential function with respect to $R_a$. The attractive interaction, $R_a$, is defined to favor the connectivity of pairs of segments. A segment $s$ has two extremities to which another segment can be connected, $U_s$ and $V_s$ (see Fig.1(a)). An attractive region $W_a$ is defined for each segment. This region is represented by disks centered at two extremities of a segment: $W_a(s) = C_a(U_s, r_a = l_s/4) \cup C_a(V_s, r_a = l_s/4)$. Fig.1(a) illustrates this definition. Two segments $s_i = (p_i, m_i)$ and $s_j = (p_j, m_j)$ have attractive interaction if the attractive region of the two segments intersect, i.e. $W_a(s_i) \cap W_a(s_j) \neq \varnothing$. The potential function between $< s_i, s_j > R_a$ is intersection area of the two region to that of the minimal one:

$$g_a(s_i, s_j) = \sum_{K1=U_{s_i}, V_{s_i}} \sum_{K2=U_{s_j}, V_{s_j}} \frac{A(C_a(K1) \cap C_a(K2))}{min(A(C_a(K1)), A(C_a(K2)))} \ , \qquad (5)$$

where $A(.)$ denotes the area of $(.)$. This interaction describes the connectivity of segments and is assigned a negative weight $\lambda_a$ to favor connectivity of segments.

Fig.1(b) shows the attractive interactions between several segments. Two segments with the minimal energy state ($g_a = 1$) defined by above potential function may take on different orientation relation of them, or different curvature. The real vessel structure will prefer $< s_1, s_2 > R_a$ to $< s_1, s_3 > R_a$ (see Fig.1(b)). We define rejective interaction to distinguish the connected segments having different orientation consistency. A rejective region $W_r(s)$ is defined for each segment: $W_r(s) = C_r(P_s, r_r = l_s/2)$. Two segments $s_i = (p_i, m_i)$ and $s_j = (p_j, m_j)$ have rejective interaction if the rejective region of the two segments intersect, i.e. $W_r(s_i) \cap W_r(s_j) \neq \varnothing$. The potential function for rejection interaction between $< s_i, s_j > R_r$ is:

$$g_r(s_i, s_j) = \frac{A(W_r(s_i) \cap W_r(s_j))}{min(A(W_r(s_i)), A(W_r(s_j)))} \ , \qquad (6)$$

with $A(.)$ being the area of $(.)$ also. This definition is also applicable to the segments which are not connected. Fig.2(a) shows the rejective region of a segment and (b) shows several examples of rejection configuration.

Similar segment process is devised and used to extract line network from remotely sensed image in [20]. Except the slight difference of the property of expected object, a distinct peculiarity of the proposed model in this paper is that no threshold for orientation is used to forbid any unexpected configuration.

### 2.2 The Data Term

To check the fitness of a segment $s$ to the data, we consider the set of pixels $Q_s$ covered by $s$ in the image. Data potential is defined with the vesselness of $Q_s$ computed by a multiscale vessel enhancement measure, based on the work of [4] on ridge filters. Having extracted the two eigenvalues of the Hessian matrix

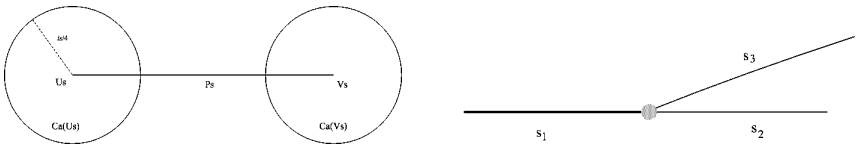


(a) (b)

**Fig. 1.** Attractive interaction of segments. (a) A segment $s$ has two extremity $U_s$ and $V_s$, and two disk attractive region centered at $U_s$ and $V_s$. (b) Three segments $s_1$,$s_2$,$s_3$ share a common endpoint, and both $g_a(s_1, s_2)$ and $g_a(s_1, s_3)$ have the same attraction potential, while the two point pairs have different consistency of orientation.

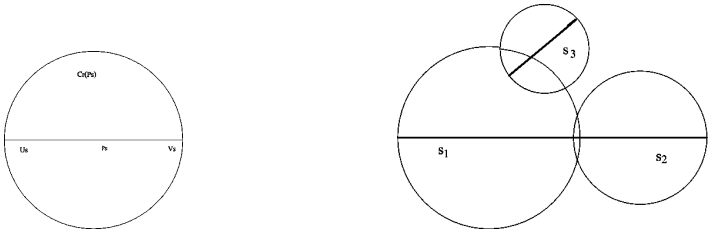


(a) (b)

**Fig. 2.** Rejective interaction of segments (a) A segment $s$ has one disk rejective region centered at $P_s$. (b) $g_r(s_1, s_2)$ and $g_r(s_1, s_3)$ have different potential values.

computed at scale $\sigma$, ordered $|\lambda_1| \leq |\lambda_2|$, a vesselness function is defined at each pixel:

$$\nu(\sigma) = \begin{cases} 0, & \text{if} \lambda_2 \geq 0 \\ \exp \frac{-R_B^2}{2\beta^2}(1 - \exp \frac{-S^2}{2c^2}), & \text{otherwise} \end{cases} . \tag{7}$$

where $R_B = \frac{|\lambda_1|}{|\lambda_2|}$, and $S = \sqrt{\lambda_1^2 + \lambda_2^2}$. A detailed explanation of each parameter in this measure is in [4]. A vesselness image can be taken with the maximum of the response of the filter across several selected scales. We expect that the pixels in $Q_s$ have big vesselness, thus define the data energy of the point process $S$ as

$$E_d(S) = \lambda_d \sum_{s \in S} \psi(\nu(Q_s)) \ . \tag{8}$$

$\nu(Q_s)$ is the mean vesselness of all the pixels in $Q_s$. $\psi(x) = (\frac{1-x}{1+x})^k$ is a decreasing function. This function casts a range (depending on $k$) of vesselness into energy near zero.

### 2.3 Optimization by Data-Driven MCMC

A solution for the point process is represented by a point set

$$S = (N, \{(x_i, y_i), l_i, \Theta_i\}; i = 1, 2...N) \ , \tag{9}$$

where the number of point $N$ is unknown and the solution space is a union of many subspaces $\Omega_N$ of varying dimensions:

$$\Omega = \cup_{N=0}^{\infty} \Omega_N, \Omega_N = \wedge \times \Omega_M \ , \tag{10}$$

where $\Omega_N$ is the subspace with exactly $N$ point. It is further decomposed into location and marker space.

**Designing Ergodic Markov Chain Dynamics.** The search algorithm should make the markov chain can visit any state in the solution in finite time steps. It requires both jump dynamics which move between subspace of varying dimensions and diffusion dynamics which move within a subspace of a fixed dimension. That the Markov chain have $f(S)$ as its invariant probability at equilibrium is assured by detailed balance at every move and the reversibility of each move.

We use the Reversible Jump Markov Chain Monte Carlo (RJMCMC) algorithm with a Metroplis-Hasting-Green dynamics [11],[12] to simulate the process distribution $f(S,T)$ specified by the density $[f(S)]^{\frac{1}{T}}$. At any state of the Markov chain, a propose kernel is proposed and the transition is accepted with a probability given by the Green's ratio. This accepted rate is computed so that the detailed balance condition is verified, condition under which this algorithm converge to $f(S,T)$.

We adopt three types of dynamics in the evolution of Markov chain, which are used randomly with probabilities $q_b$, $q_d$, $q_m$ respectively.

*Dynamics 1: Birth of a point.* It is a process of jump between spaces of different size. Suppose at a certain time step, we propose to birth a point, thus move the Markov chain from current state $S$ to $S \cup \{s'\}$. By the classic Metropolis-Hastings method [21], we need two proposal probabilities $p(S \to S \cup \{s'\})$ for the move and $p(S \cup \{s'\} \to S)$ for moving back. Then the proposal move is then accepted with probability

$$\alpha(S \to S \cup \{s'\}) = min(1, \frac{p(S \cup \{s'\} \to S) f^{\frac{1}{T}}(S \cup \{s'\})}{p(S \to S \cup \{s'\}) f^{\frac{1}{T}}(S)}) \ . \tag{11}$$

*Dynamics 2: Death of a point.* It is the reversible jump of Dynamics 1. In this case of death of a segment $s'$, the probability to accept is

$$\alpha(S \to S \setminus s') = min(1, \frac{p(S \setminus s' \to S) f^{\frac{1}{T}}(S \setminus s')}{p(S \to S \setminus s') f^{\frac{1}{T}}(S)}) \ . \tag{12}$$

*Dynamics 3: Diffusion of the length and orientation of a point.* It is the modification of a randomly chosen object according to a symmetrical transformation. The transformation can be stretching of length or changing the orientation of the considered segment:

$$S \to (S \setminus s(p_s, l_s, \theta_s)) \cup \{s'(p_s, (l_s + d_l)[l_{min}, l_{max}], \theta_s + d_\theta[0, \pi])\} \ , \tag{13}$$

where [.] denotes the module function. $d_{(.)}$ is a small step of (.). The acceptance probability for this dynamic is

$$\alpha(S \rightarrow (S \setminus s) \cup \{s'\}) = min(1, \frac{f^{\frac{1}{T}}((S \setminus s) \cup \{s'\})}{f^{\frac{1}{T}}(S)}) \ . \tag{14}$$

**Computing Important Proposal Probabilities in Cue Space.** The effectiveness of MCMC depends critically on the design of the proposal probability. The important proposal probability can be computed using Data-Driven methods [13]. We use the computation of vesselness, presented in section 2.2 for data term, to define a birth kernel.

To compute $p(S \rightarrow S \cup \{s'\}$ in formula (11), the route first chooses a birth move with probability $q_b$, then chooses a point $p_i$ from the pixel domain $\wedge$; this probability is denoted by $q(p_i)$. Given $p_i$, it chooses a length $l_i$ and an orientation $\theta_i$ with probabilities $q(l_i|p_i)$ and $q(\theta_i|p_i)$ respectively. Thus,

$$p(S \rightarrow S \cup \{s'\}) = q_b q(p_i) q(l_i|p_i) q(\theta_i|p_i) \ . \tag{15}$$

$q(p_i)$ is often decided by the goodness of fit on a point. A point with good fit has a higher chance to birth. From the vesselness computed in section 2.2 of each point, we can define an inhomogeneous birth kernel for the midpoint coordinate of a segment

$$q(p_i) = \frac{\nu(p_i)}{\sum_{p_j \in \wedge} \nu(p_j)} \ , \tag{16}$$

where $\nu(p_i)$ is the vesselness of point $p_i$. Similarly, we can also define an inhomogeneous kernel for the orientation given the segment midpoint. It is computed by the mean vesselness of a segment under all the possible orientation with a fixed length. Lastly, $q(l_i|p_i)$ is the uniform distribution in the length space.

The proposal probability for a death move is

$$p(S \cup \{s'\} \rightarrow S) = q_d \frac{1}{n(S)+1} \ , \tag{17}$$

where $n(S)$ is the number of segments in $S$. It means choosing a point in the current configuration randomly under uniform distribution for a death move.

## 3 Experiments on Simulation of the Point Process

The proposed method is implemented on the clinical coronary and some of the results are reported in this section. Fig.3(a) is a part of original angiogram. The minimal and maximal diameter of vessel tree is about 5 and 17 pixels respectively. We use three scale, $\sigma$ being 2, 4, 8, respectively, to compute the vesselness image by formula (7). Fig.3(b) shows the result of this vesselness filter. The normalized vesselness image is treated as a distribution for the proposal probability for birth a segment, which is expressed by formula (16). The proposal probability of the orientation given a point also is computed from the vesselness image. Fig.3(c)

is the result of simulation of the point process. The interaction parameters were fixed to $\lambda_0 = 1$, $\lambda_1 = 0.7$, $\lambda_2 = 0.4$, $\lambda_a = 1.75$, $\lambda_r = 5.5$, $\lambda_d = 0.9$.

Other results are shown in Fig.4; (a) and (d) are the original angiogram; (b) and (e) are the extracted approximate centerline by the point process; (c) and (f) are the results of segmentation by watershed, which will be presented in next section. It can be seen that some small branching of vessel is missed by the point process in (e). It shows that there is need for more consideration for the parameter to balance the prior and data term.

## 4 Extraction of Coronary Artery Edge with Marker Watershed

The centerline extracted above provides important clues of form as well as locations of vessel and many local operators can be used to detect the accurate vessel boundary based on it. Though the gray intensity of background varies on the angiogram, there exists gray level different between the vessel and the background everywhere. The implementation of morphological watershed transform on gradient image of original angiogram can extract the watershed lines (vessel boundary) which separate the homogeneous gray region [22]. Oversegmentation is prevented by only using the regional minima defined by the centerline.

The edge extraction process is implemented on each branching of centerline respectively. Fig.5(a) is a branching of centerline, which acts as the vessel marker. Then dilating of it produces the marker of background. See the blank region in Fig.5(b). Then obtained marker of vessel and background is lastly used to modify gradient image of original angiogram, and the edge of vessel is achieved by watershed on the modified gradient image. Fig.5(c) is the morphological gradient image of part region in original image of Fig.3(a). Fig.5(d) is the gradient image with the region of vessel marker and background marker being zero. The suppression of the minima not related to the markers is achieves by applying geodesic reconstruction techniques [23] [24]. Fig.5(e) shows the modified gradient image with such operator. Taking watershed operator on Fig.5(e) get the edge of vessel shown in Fig.5(f). Union of the result of each branching produces the last vessel segmentation result shown in Fig.3(d) imposed on original angiogram. The results of the other two angiogram are shown in Fig.4(c) and (f).

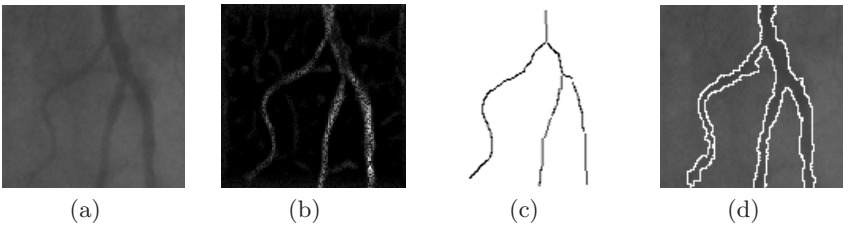

(a) (b) (c) (d)

**Fig. 3.** Approximate centerline extraction. (a) Original angiogram. (b) Vesselness image. (c) Approximate centerline. (d) Edges imposed on original image.

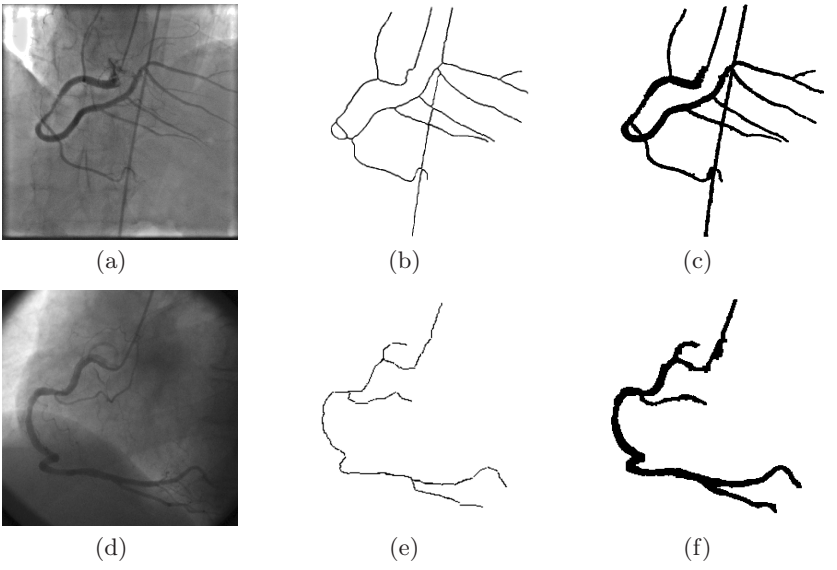


**Fig. 4.** (a),(d) Original angiogram. (b),(e) Extracted approximate centerline. (c),(f) Segmentation result.

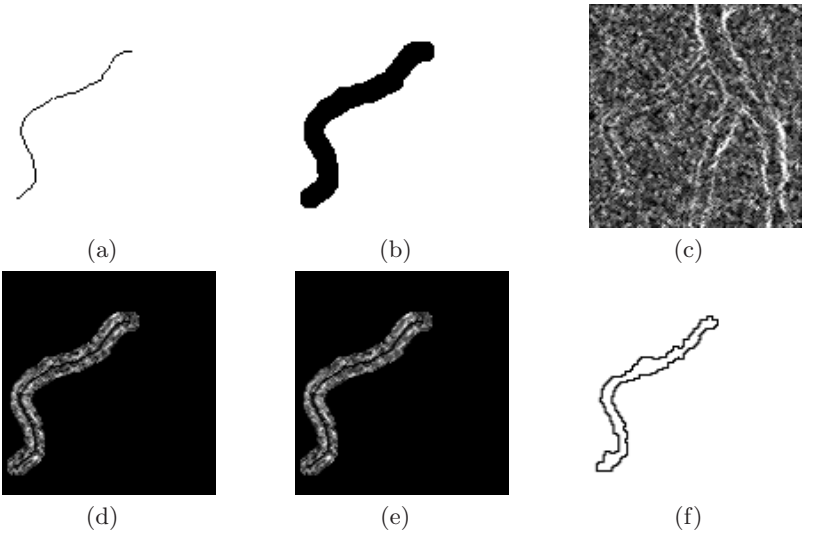


**Fig. 5.** (a) Centerline as vessel marker. (b) Dilation of (a) as background marker. (c) Gradient image of Fig.1(a). (d) Gradient image with vessel and background marker region being zero. (e) Gradient image with local minimum modified. (f) Extracted vessel edge by watershed.

## 5 Discussion

In this paper, we show a method to obtain the important information of the shape and the location of the coronary artery tree by the marked point process. The accurate edge is obtained with local operator guided by the shape and location information.

The properties of the proposed prior model need to be more deeply investigated. Relevant moves require to be defined to accelerate the convergence of the Markov chain. We use a simple measure for the data likelihood in this paper. However, many existed methods for vessel extraction may be used to compute important probabilities and data energy term. When the vessel structure takes on vessel very complex curvature relation, the ability of the proposed point process will be restricted by the length space of the segment. A possible method solving this problem is to generalize the segment process into the pure curve process, which is nearer to the real vessel structure than line segment.

**Acknowledgments.** This work was supported by 973 Program of China (No: 2003CB716105).

## References

1. Sorantin, E., Halmai, C., Erbohelyi, B., Palagyi, K., Nyul, K., Olle, K., Geiger, B., Lindbichler, F., Friedrich, G., Kiesler, K.: Spiral-CT-based assesment of Tracheal Stenoses using 3D Skeletonization. IEEE Trans. Med. Imag. 21, 263–273 (2002)
2. Eberly, D., Gardner, R.B., Morse, B.S., Pizer, S.M., Scharlach, C.: Ridges for image analysis. JMIV 4, 351–371 (1994)
3. Wink, O., Niessen, W.J.: Max, A.: Viergever. Multiscale Vessel Tracking. IEEE Trans. Med. Imag. 23 (January 2004)
4. Frangi, A.F., Niessen, W.J., Vincken, K.L., Viergever, M.A.: Vessel enhancement filtering. In: Proc. Medical Image Computing and Computer- Assisted Intervention, pp. 130–137 (1998)
5. Sato, Y., Nakajima, S., Shiraga, N., Atsumi, H., Yoshida, S., Koller, T., Gerig, G., Kikinis, R.: 3d multi-scale line filter for segmentation and visualization of curvilinear structures in medical images. Medical Image Analysis 2, 143–168 (1998)
6. Quek, F., Kirbas, C.: Vessel extraction in medical images by wave propagation and traceback. IEEE Trans. on Med. Img. 20, 117–131 (2001)
7. Nain, D., Yezzi, A., Turk, G.: Vessel Segmentation Using a Shape Driven Flow. In: Medical Imaging Copmuting and Computer-Assisted Intervention (2004)
8. Kass, M., Witkin, A., Terzoopoulos, D.: Snakes: Active contour models. Int. J. of Comp. Vision 1, 321–331 (1988)
9. Caselles, V., Catte, F., Coll, T., Dibos, F.: A geometric model for active contours in image processing. Numerische Mathematik 66, 1–32 (1993)
10. van Lieshout, M.: Markov Point Processes and Their Applications. Imperial College Press (2000)
11. Geyer, C.J., Møler, J.: Simulation and Likelihood Inference for Spatial Point Process. Scandinavian J. Statistics, Series B 21, 359–373 (1994)

12. Green, P.: Reversible Jump Markov Chain Monte-Carlo Computation and Bayesian Model Determination. Biometrika 57, 97–109 (1995)
13. Tu, Z.W., Zhu, S.C.: Image segmentation by data-driven Markov chain Monte Carlo. IEEE Trans. Pattern Anal. Machine Intell. 24, 657–673 (2002)
14. Thönnes, E., Bhalerao, A., Kendall, W., Wilson, R.: A Bayesian Approach to inferring vascular tree structure from 2D imagery. In: Proceedings of IEEE ICIP, Rochester, New York, vol. II, 937–939 (2002)
15. Lacoste, C., Finet, G., Magnin, I.E.: Coronary Tree Extraction from x-ray Angiograms using Marked Point Process. In: Proceedings of IEEE ISBI, Arlington, Virginia, pp. 157–160 (2006)
16. Baddeley, A.J., van Lieshout, M.N.M.: Stochastic geometry models in high-level vision. In: Mardia, K.V., Kanji, G.K. (eds.) Statistics and Images, (Advances in Applied Statistics, a supplement to Journal of Applied Statistics), Nashville, TN, Abingdon, vol. 1, pp.231–256 (1993)
17. Zhu, S.C.: Statistical modeling and conceptualization of visual patterns. IEEE Trans. Pattern Anal. Machine Intell. 25, 691–712 (2003)
18. Geman, S., Geman, D.: Stochastic Relaxation, Gibbs Distributions, and the Bayesian Restoration of Images. IEEE Trans. Pattern Anal. Machine Intell. 6, 721–741 (1984)
19. Stoica, R., Descombes, X., Zerubia, J.: A Gibbs Point Process for Road Extraction in Remotely Sensed Images. Int'l J. Computer Vision 57(2), 121–136 (2004)
20. Lacoste, C., Descombes, X., Zerubia, J.: Point Processes for Unsupervised Line Network Extraction in Remote Sensing. IEEE Trans. Pattern Anal. Machine Intell. 27, 1568–1579 (2005)
21. Metropolis, N., Rosenbluth, M.N., Rosenbluth, A.W., Teller, A.H., Teller, E.: Equations of State Calculations by Fast Computing Machines. J. Chemical Physics 21, 1087–1092 (1953)
22. Vincent, L., Soille, P.: Watersheds in digital spaces: An efficient algorithm based on immersion simulations. IEEE Trans. Pattern Anal. Machine Intell. 13(6), 583–598 (1991)
23. Vincent, L.: Morphological grayscale reconstruction in image analysis: Applications and efficient algorithms. IEEE Trans. Image Processing 2(8), 176–201 (1993)
24. Haris, K., Efstratiadis, S., Maglaveras, N., Pappas, C., Gourassas, J., Louridas, G.: Model-Based Morphological Segmentation and Labeling of Coronary Angiograms. IEEE Trans. Med. Imag. 18(10), 1003–1015 (1999)